Relationships between Gravity Waves Observed at Earth's Surface and in the Stratosphere over the Central and Eastern United States

Catherine D. de Groot-Hedlin[1], Michael A.H. Hedlin[1], Lars Hoffmann[2],
M. Joan Alexander[3] and Claudia C. Stephan[4]

[1] Laboratory for Atmospheric Acoustics, Institute of Geophysics and Planetary Physics, Scripps Institution of Oceanography, University of California, San Diego

[2] Jülich Supercomputing Centre, Forschungszentrum Jülich, Jülich, Germany

[3] NorthWest Research Associates, Inc., CoRA Office, Boulder, Colorado

[4] National Centre for Atmospheric Science - Climate, Department of Meteorology, University of Reading, Reading, UK

corresponding author: Catherine de Groot-Hedlin

Key Points:

1) A gravity wave hotspot is detected on the Earth's surface west of the Great Lakes using the USArray Transportable Array barometric network.

2) Gravity wave occurrence rates on the ground exhibit the same broad spatial and temporal patterns as observed at stratospheric altitudes.

3) Evidence suggests that convective activity is the dominant source of gravity waves both at the ground and in the stratosphere.

Abstract

Observations of tropospheric gravity waves (GWs) made by the new and extensive USArray Transportable Array (TA) barometric network located east of the Rockies, in the central and eastern United States and of stratospheric (30-40 km above sealevel) GWs made by the Atmospheric InfraRed Sounder (AIRS) are compared over a 5-year time span from 2010 through 2014. GW detections in the period band from 2-6 hours made at the Earth's surface during the thunderstorm season from May through August each year exhibit the same broad spatial and temporal patterns as observed at stratospheric altitudes. At both levels, the occurrence frequency of GWs is higher at night than during the day and is highest to the west of the Great Lakes. Statistically significant correlations between the variance of the pressure at the TA, which is a proxy for GWs at ground level, with 8.1 μm brightness temperature measurements from AIRS and rain radar precipitation data, which are both proxies for convective activity, indicate that GWs observed at the TA are related to convective sources. There is little, if any, time lag between the two. Correlations between GWs in the stratosphere and at ground level are weaker, possibly due to the AIRS observational filter effect, but are still statistically significant at nighttime. We conclude that convective activity to the west of the Great Lakes is the dominant source of GWs both at ground level and within the stratosphere.

1. Introduction:

Atmospheric gravity waves (GWs) are a significant driver of global-scale atmospheric circulation and substantially impact weather and climate. They commonly originate in the troposphere, where they are generated by a variety of sources including convective storm systems. Many observational studies have shown the close correspondence of GWs with deep convective clouds. Reports of GWs observed in surface pressure observations date back to the 1940s and 50s (Brunk 1949; Tepper 1954), but research on these waves and their interactions with convective storms languished until a revival in the 1970s (Bosart and Cussen 1973; Eom 1975; Ucellini 1975). GWs in the stratosphere have been tied to convective storms in early case studies (e.g. Larsen et al. 1982; Pfister et al. 1986; Alexander and Pfister 1995) and more recently in climatological studies with satellite observations from the Atmospheric Infrared Sounder instrument (Hoffmann and Alexander 2010; Gong et al. 2012; Choi et al. 2012; Hoffmann et al. 2013; Tsuchiya et al. 2016; Sato et al. 2016). GWs near the surface can initiate or intensify convective storms (e.g. Stobie et al. 1983; Mapes 1993), and stratospheric GWs can influence general circulation, particularly in the tropics and summer hemisphere (e.g. Alexander and Rosenlof 1996; Scaife et al. 2000).

The Atmospheric Infrared Sounder (AIRS) is a nadir sounder, sensitive to GWs with long vertical wavelengths and short horizontal wavelengths. Nadir sounders provide good horizontal resolution of long vertical wavelength GWs, which can cause significant wave drag and carry large momentum flux (Eckermann et al. 2006; Wu et al. 2006; Alexander and Barnet 2007; Preusse et al. 2008). In addition to the climatological studies mentioned above, AIRS data have been applied to case studies of convective GWs related to deep convection, storms, and hurricanes (Grimsdell et al., 2010; Choi et al., 2012; Yue et al. 2014; Stephan and Alexander, 2015). Many observational studies have shown the close correspondence of GWs with deep convective clouds. The climatology study of Hoffmann and Alexander (2010) demonstrated that GW occurrence in North America is closely associated with regions of thunderstorm activity. The most active region in North America is located over the Great Plains to the west of the Great Lakes. Most of these GWs are associated with deep convection (Hoffmann and Alexander, 2010). Convective GWs are most commonly observed by AIRS during local night during the thunderstorm season from May to August.

Although there has been significant progress in observing GWs in the middle atmosphere using space-based sensors, it is unclear whether or how GWs observed at the Earth's surface are generally related to those observed in the stratosphere. Investigations of mesoscale pressure fluctuations, including gravity waves, at Earth's surface include studies at a small network, comprising 6 or 7 barometers with a 2 minute sampling rate within a 50 km radius (Grivet-Talocia and Einnaudi, 1998; Grivet-Talocia et al., 1999), and another network with several hundreds of stations with 5 to 15 minute sampling rates spanning the continental United States (Koch and Handley, 1997; Koppel et al., 2000; Koch and Saleeby, 2001). Pressure observations from a large network of barometers that were deployed within the continental US as one component of the USArray Transportable Array (TA) are used in this study. The barometric component of the TA comprises 400 identical sensors that provide pressure data with high temporal resolution, deployed in a Cartesian-like grid (Tytell et al., 2016; Jacques et al., 2016). The nearly uniform station distribution (~70 km interstation spacing) and high time sampling rate enables the use of array processing techniques to detect and characterize mesoscale pressure perturbations on a large scale. This allows us to use barometric data to further our understanding of how GWs in the troposphere relate to those observed in the stratosphere. The TA barometric network has previously been used to study GWs that originated near a severe tornadic storm system in the southern US (de Groot-Hedlin et al., 2014). In a case study, Stephan et al. (2016) linked TA surface pressure oscillations and GWs observed in the stratosphere to a common precipitating storm source using radar observations and the idealized GW-resolving method of Stephan and Alexander (2015). In other studies, Jacques et al., (2015, 2017) used this network to identify mesoscale pressure fluctuations.

In this study, we examine links between surface waves and stratospheric waves more generally. We apply a GW detection method to data recorded by the TA network to compile statistics on GW occurrence and wave properties at ground level for comparison with corresponding observations of GWs in the stratosphere made by the AIRS instrument. The study area spans the eastern half of the continental United States and compiles observations made over a 5-year timespan from the beginning of 2010 to the end of 2014. This study addresses how GW occurrence rates vary geographically, diurnally and seasonally across this region, with a particular focus on the thunderstorm seasons each year. In addition to the large-scale analysis, data recorded during the thunderstorm season in 2011 from the hotspot located to the west of the Great Lakes are examined in greater detail to determine whether there is any correlation from day to day between the rate of occurrence of GWs on the ground, deep convection events, the background winds, and the occurrence of GWs in the stratosphere.

The paper is organized as follows. The datasets are described in Section 2. Section 3 outlines a method for detecting GWs using TA data, and presents the occurrence rate at the Earth's surface over a 5 year period from 2010-2014. In section 4, observations of GWs and deep convection in the stratosphere made by the AIRS instrument are described. We discuss the spatial and temporal correlation of GWs in the stratosphere and Earth's surface in section 5. A discussion and conclusions are presented in section 6.

2. Data:

2.1 Pressure data

The USArray Transportable Array (TA) originated as a broadband seismic experiment on the west coast of the continental United States in 2004 (Busby et al., 2006). By late 2007 the network included approximately 400 stations that were deployed in a Cartesian-like grid with sites located nearly every 70 km along north-south and east-west lines across a region covering approximately 2,000,000 km^2. Each station was deployed for two years, after which the equipment was transferred from the western edge to a new location at the eastern edge of the network. In this manner, the network gradually moved east across the continental US, reaching the Atlantic coast in 2013. The network was largely removed from the continental US by late 2015 with most stations being re-deployed in a less dense (85 km spaced) configuration in Alaska and Canada's Yukon territory.

Beginning in 2009, atmospheric packages were added to each new station in the network. This package included a micro-electromechanical system (MEMS) pressure sensor (sensitive from DC to 100 s), a Setra 278 (DC to 1 Hz) and a Hyperion high-frequency infrasound microphone (sensitive from 200 s to above the Nyquist frequency). A map of the upgraded stations, shown in Figure 1, shows the change in the location of the network over time since the upgrade began. In total, over 1,000 sites were occupied in the continental US. Data from all stations are digitized at 1 Hz for the MEMS sensors and 40 Hz for the other sensors, then telemetered in near-realtime to the Array Network Facility (ANF) at UC San Diego for preliminary processing before being forwarded to the Data Management Center (DMC) in Seattle, WA where they are archived and made available to the general public. The 1 Hz data are also archived in the Research Data Archive at the National Center for Atmospheric Research Jacques et al., 2016). The installation of MEMS sensors began several months before the other sensors. Since MEMS data are available at more sites than the other sensors, and have a sufficiently broad frequency range, they were used for this study. Given the average station spacing of 70 km, coherent signals with horizontal wavelengths greater than 140 km can be observed by this network. The 1 Hz temporal sampling rate allows for the detection of signals with phase speeds up to thousands of m/s, although the GW signals observed in this study have phase velocities of several tens of m/s.

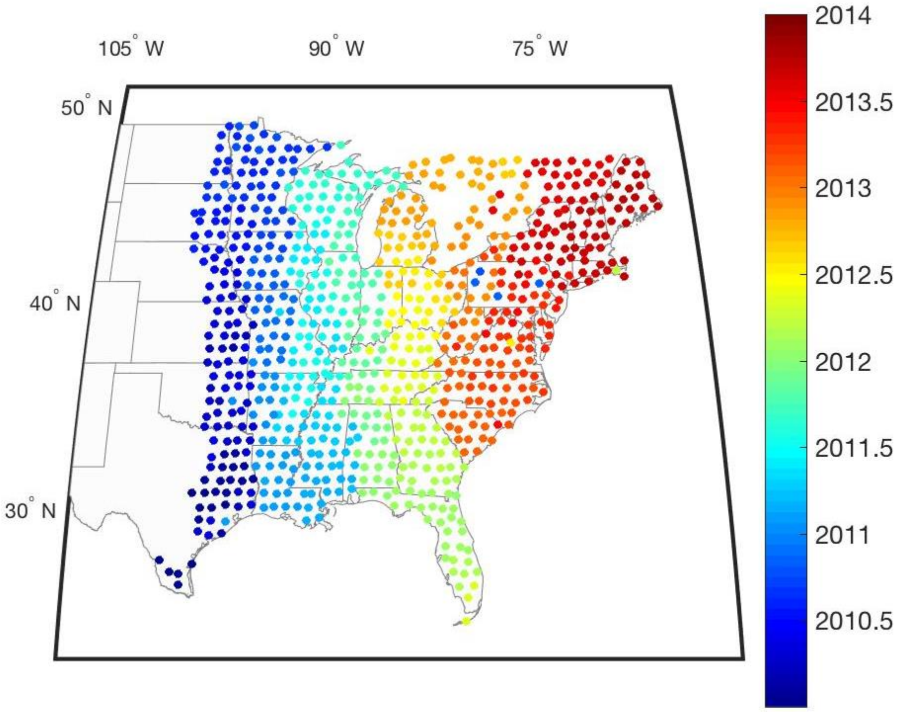

Figure 1. Deployment of stations in the TA that include MEMS sensors. Stations are color coded by the date they began operating. Each station was left in place for approximately two years before being moved from the west to the leading (eastern) edge of the network.

Many physical processes that occur simultaneously affect the barometric pressure at different temporal and spatial scales. As for most types of geophysical measurements (Agnew, 1992), the barometric pressure data at each TA station has a “red” spectrum, which means that the energy at long periods exceeds that at shorter periods. This holds true over a wide range of frequencies. For instance, Jacques et al., (2015) observed that the average variance of barometric pressure signals at the TA in the 30 h to 5 day band were an order of magnitude greater than variances in the 4 h to 30 h band, and over two orders of magnitude greater than variances in the 10 min to 4 h band. Pressure perturbations in these bands ranged from hundreds to thousands of pascals. In contrast, infrasound signals from the Chelyabinsk meteor event with amplitudes as low as 1 Pa were detectable at the TA at periods ranging from 8 to 125 s, (de Groot-Hedlin and Hedlin, 2014). Figure 2 is a map of unfiltered barometric pressure data at the northern end of the TA at 0700 UT on June 27, 2011, with long-term, altitude-dependent, pressure removed at each station. As shown, the TA extends about 23^{o} in latitude and 13^{o} in longitude at this time.

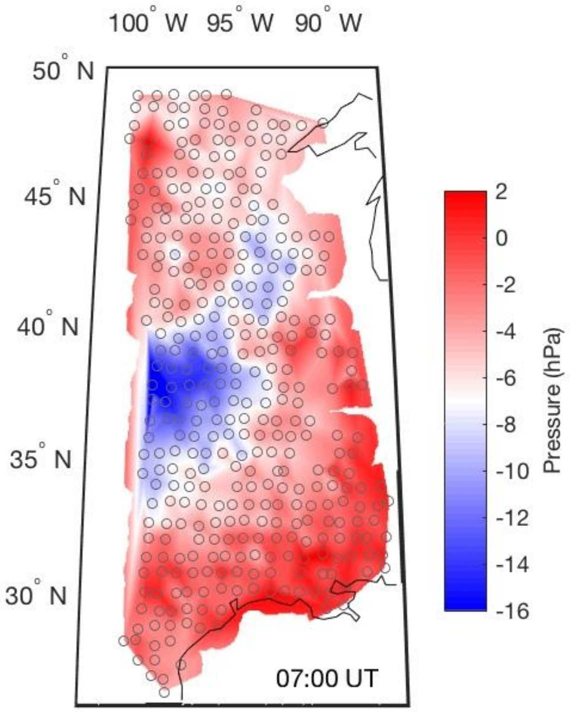

Figure 2. Map of the pressure variations (in hPa) at 0700 UT on June 27, 2011, with long-term mean pressure removed. The pressure at each station, shown by the open circles, are spatially interpolated.

2.2 Satellite data

The AIRS sensor (Aumann et al., 2003; Chahine et al., 2006) is located aboard NASA's Aqua satellite, which was launched in a nearly polar, low earth orbit in May 2002. Aqua achieves nearly global coverage during 14.4 daily orbits. The orbit is sun-synchronous, with Equator crossings at 01:30 local time (LT) (descending orbit nodes) and 13:30 LT (ascending orbit nodes). AIRS measures infrared radiance spectra from the Earth's atmosphere in the nadir and sub-limb geometry.

Information on GW activity is inferred from AIRS radiance measurements using the approach of Hoffmann and Alexander (2010) and Hoffmann et al. (2013, 2014). Spectral mean brightness temperatures (BTs) are analyzed in the 4.3 μm CO_2 fundamental band, which gets optically thick in the mid-stratosphere at about 30-40 km altitude. The spectral mean kernel functions of the selected AIRS channels are rather broad, with a full width at half maximum of about 25 km. The AIRS measurements are most sensitive to GWs with vertical wavelengths longer than 25 km, but moderate sensitivity is found for vertical wavelengths as short as 10-15 km. There are three main contributions to the observed BT: (i) GW signals, (ii) background signals varying on large scales, and (iii) measurement noise. The detrending procedure of Alexander and Barnet (2007) is used to remove the background signals associated with large-scale temperature gradients and limb brightening. The detrended BT perturbations are most sensitive to GWs with horizontal wavelengths shorter than 730 km. Given the footprint size of the satellite scans, the lower horizontal wavelength limit of the GW observations is about 30 km. The 4.3 µm BT variances shown in this paper have been corrected for noise by subtracting noise variances scaled to scene temperature.

As an example, Figure 3 shows AIRS observations of stratospheric GWs over the North American Great Plains on 27 June 2011. Measurements are shown for the descending parts of the satellite orbits, which are nighttime measurements. The 4.3 µm BT perturbation map reveals significant GW activity to the southwest of the Great Lakes. The AIRS observations show semi-circular wave fronts/patterns to the east of the convective sources. Wave patterns to the west of the convective sources are not observed by AIRS. The east-west difference is predominantly due to the prevailing easterly background winds, causing Doppler-shifting towards long vertical wavelengths in the east and short vertical wavelengths in the west. GWs with long vertical wavelengths are more clearly visible to AIRS due to the nadir observation geometry. Short-scale waves with horizontal wavelengths of less than about 100 km are found close to the convective sources whereas larger-scale waves are found at greater distances, having propagated further from the convective sources. This is consistent with linear wave theory and the horizontal wavelength dependence of horizontal group velocity. Propagation of the convective sources, and filtering by the background wind, which occurs when a wave approaches a level where the wave phase speed equals the wind speed, may additionally contribute to the observed east-west asymmetry.

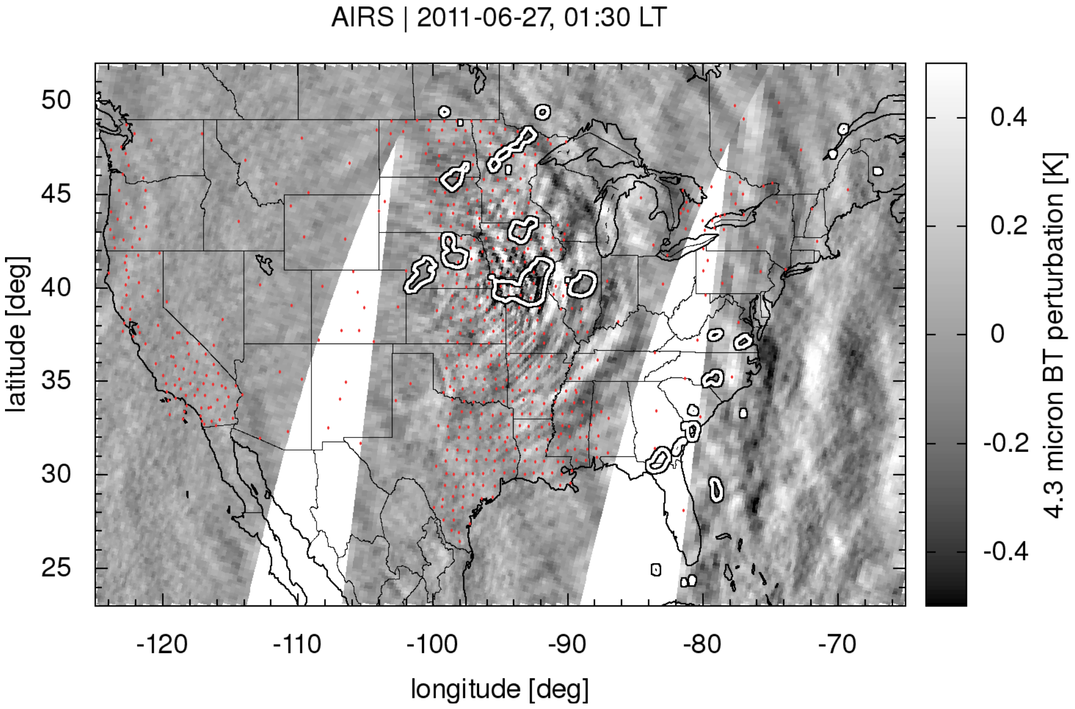

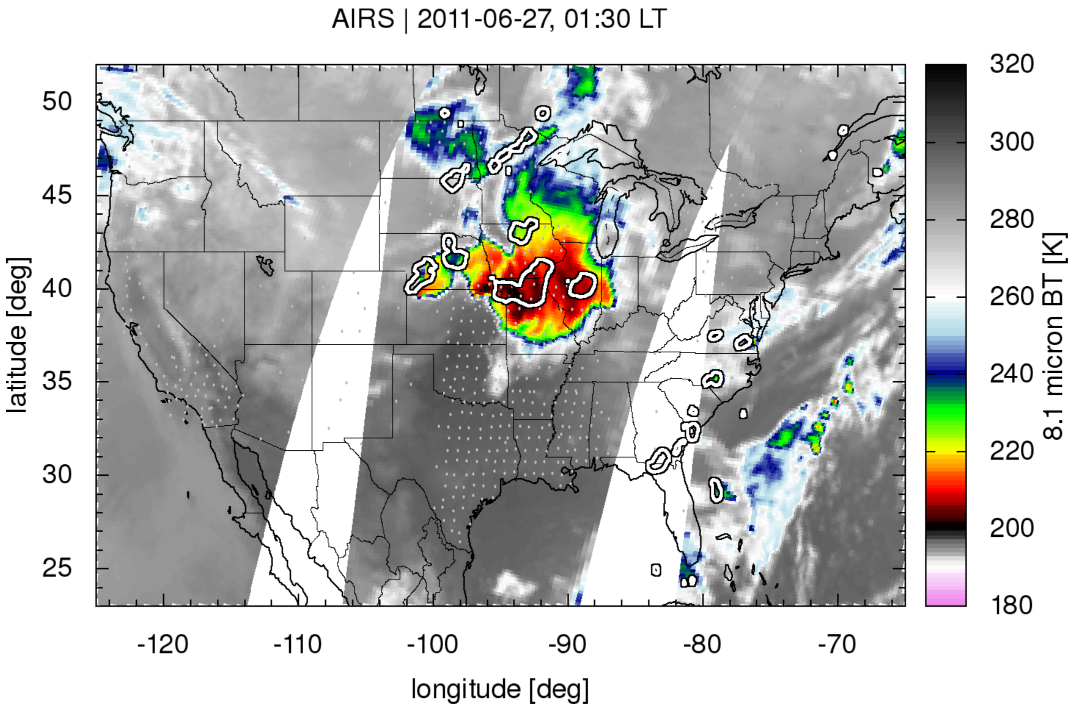

Figure 3. The upper and lower panels show BT perturbations in the 4.3 µm spectral region and BTs in the 8.1 µm spectral region, respectively. These images were taken from AIRS radiance measurements on June 27, 2011 during the night-time, descending orbit. Contour lines in both panels show 6 mm/hr maximum precipitation rates for 0700 UT. The small dots show the TA station locations on that date.

2.3 Precipitation data

The National Centers for Environmental Prediction/Environmental Modeling Center's (NCEP/EMC) gridded Stage IV precipitation data is a mosaic produced from radar observations. It is based on the multi-sensor hourly Stage III analysis produced by the 12 River Forecast Centers in the continental U.S. After a manual quality control performed at the River Forecast Centers it is made into a national product. The dataset is available from 1 Jan 2002 onwards on a polar-stereographic grid with a resolution of 4.7625 km at 60° N. For this study the average and maximum precipitation rate are computed on a coarse grid, where each coarse grid box is formed of 7x7 Stage IV grid cells.

3. GW observations at Earth's surface

3.1 Detection method for GWs

The configuration the TA network allows for the detection of pressure perturbations with wavelengths greater than 140 km, and observation of how the properties of these signals change with time and location. Data from this network were used by de Groot-Hedlin et al., (2014) to track the motion of GWs generated near a convective storm system across the US. The study showed that, given the geometry of the TA and the amplitude spectrum of the observed GWs, signals with periods of several hours could be followed.

Eom (1975) found that GWs observed on surface pressure sensors had periods from 3 to 4 hrs. Other studies apply bandpass filters ranging from 1-5 h (Ucellini, 1975), 1-8 h (Stephan et al.,2016) and 32 min-4.5 h (Koch and Saleeby, 2001) to examine GWs. Grivet-Talocia et al., (1999) use a highpass filter with a cutoff at 6 h to measure mesoscale pressure fluctuations including GWs, and found that results were insensitive to cutoff periods up to 8 h. For this study, a period band from 2-6 hours was chosen. Given that the energy spectrum is "red" so that the energy decreases at higher frequencies, the results are insensitive to the lower end of this band. Figure 4 shows both raw and 2-6 hour bandpassed recordings made on June 27, 2011 by MEMS sensors located between longitude 93 to 94° W, the same day that the AIRS instrument detected a large signal in the stratosphere (Figure 3). The raw data show a disturbance with durations from 4 to 15 hours superimposed on gradual pressure variations. Large signals in the 2-6 hr bandpass are observed near 38-44°N between 01:00 and 13:00 UT, and are seen to be travelling to the south and north at later times. The signals are coherent between stations.

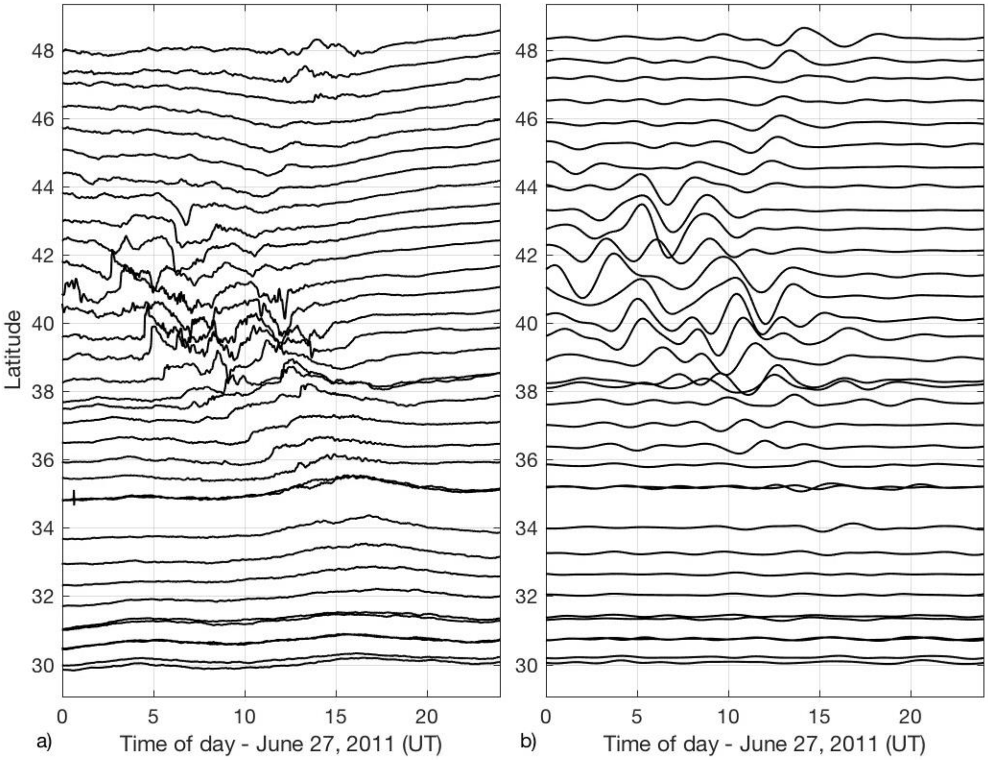

Figure 4. Record section from June 27, 2011 using stations located in a north-south column of the TA between longitudes 93° W and 94° W. Each line is a recording from a single station. a) raw data, with a scale of 800 Pa per degree latitude, b) data bandpassed from 2-6 hours using a Butterworth filter, with a scale of 400 Pa per degree latitude. Waves with amplitudes ~100Pa are observed to propagate both northward and southward from a central region near 42° N.

Figure 5 shows maps of the bandpassed pressure recordings, separated by 1 hour. These times - 0700 UT and 0800 UT - are close the time of the image from the AIRS instrument on that day (Figure 3). As shown, signal wavelengths are greater than the inter-station spacing and are coherent between stations, making them amenable to array processing to obtain estimates of their arrival time at any point in the network, phase velocity, propagation direction and amplitude. Signal motion is apparent from these two time points; in this time range, the dominant direction of motion is toward the southeast.

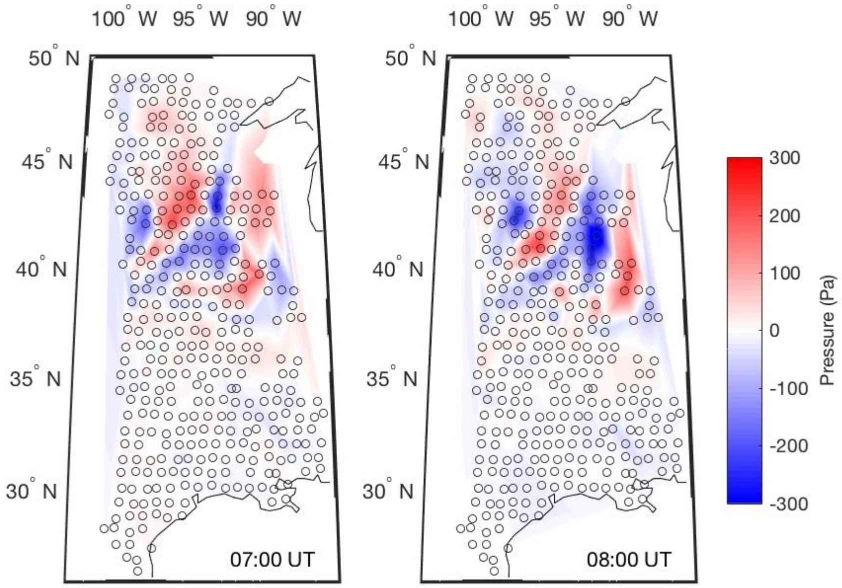

Figure 5. Maps of the pressure variations (in Pa) in the 2-6 hr band at two times (0700 and 0800 UT) on June 27, 2011. The bandpassed pressure measurements are spatially interpolated between stations, shown by the open circles.

An algorithm to detect weak, long-wavelength signals that are detectable over only a subset of sensors within a broader network, described in de Groot-Hedlin et al. (2014), is applied here to detect propagating GWs. First, the Delaunay triangulation (Lee and Schachter, 1980) is used to discretize the network into a large number of non-overlapping, adjacent arrays, each comprising three adjacent stations (called triads). For each triad, an array analysis is performed over a series of time windows of 16 hours duration, with two-hour time-steps between windows, which gives 14 hours of overlap between time windows. This temporal spacing allows for examination of diurnal variations in the GW occurrence rates. Briefly, the array analysis consists of cross-correlating the bandpassed waveforms for each of the three station pairs within each triad to find the time delays due to propagation between stations. In most cases the computed time delays around a triad are inconsistent with a single coherent signal (Cansi, 1995), and null values are retained for the signal characteristics. However, if the time delays are consistent (i.e., the signal is assumed to be consistent with a planar wavefront crossing the array), a tau-p method (Havskov and Ottemöller, 2010) is applied to the time delays to derive the signal's propagation direction and phase velocity. The high temporal sampling rate of TA data allows for accurate estimation of time delays, and hence propagation direction and phase velocity. These characteristics are used to time shift the individual waveforms measured at each sensor within the triad to bring the common signal into best alignment. The sum of these waveforms is referred to as a beam, and the process is called beamforming. The peak amplitude and corresponding arrival time of the beamformed signal are taken as additional signal characteristics, along with the phase velocity and azimuth. This analysis is repeated for each time window, for each triad within the network.

The results of these array analyses are shown in Figure 6a, for coherent signals with peak amplitudes occurring between 03:30-09:30 UT, June 27, 2011, which is local nighttime. The pressures at the Earth's surface in this time range were shown in Figure 5. Circles, color-coded by the amplitude of the beamformed signal, show where coherent GWs are detected. The arrows connected to the circles show the direction of wave propagation. In this example, the wavefront moves predominantly to the southeast. The phase velocities of the signals have a median velocity of 24 m/s, with a range from 12-96 m/s, consistent with atmospheric GW velocities.

The calculation of the occurrence frequency of GWs for any given region is complicated by the fact that the TA moved significantly to the east over the study period. To quantify the detection rate, the map area covered by the TA is gridded, with each bin extending from 0.75^{o} north-south and 1^{o} in the east-west direction, so that they are approximately square. The occurrence rate for any given bin is defined as the number of time periods in which coherent GWs are detected within that bin, divided by the number of time periods over which any triads spanned at least part of that bin. Figure 6b shows the regions in which long wavelength signals were detected, as shown in Figure 6a, and the area in which the TA resides. For any given time window, a bin is 'active' if one or more triads that lie at least partially within it detect a GW. The active bins are shown in dark red in Figure 6b. The light green bins show areas in which the TA is deployed, but no GWs are detected for this time period.

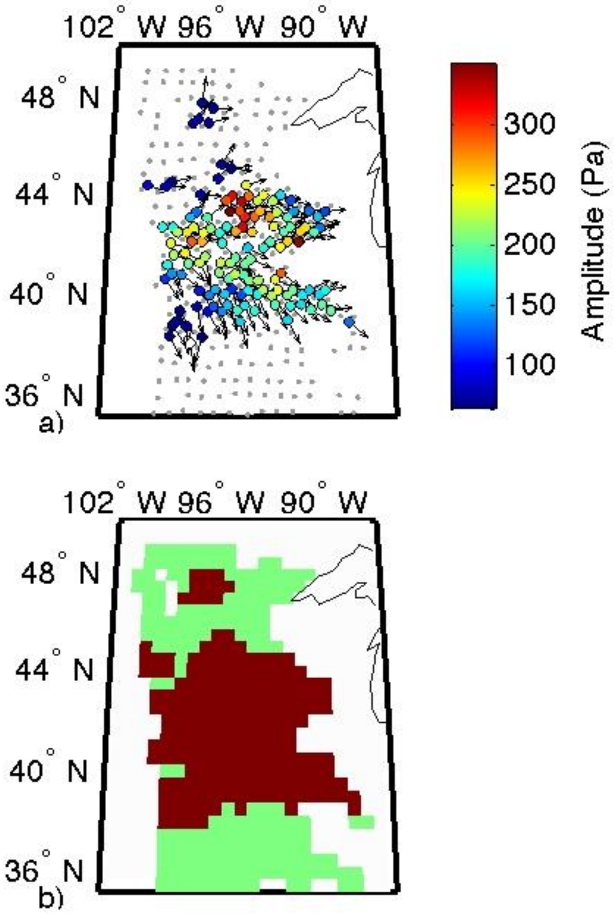

Figure 6. a) Signal pressure amplitudes and direction of motion detected at the TA within the time period from 03:30-09:30 UT on June 27, 2011, coinciding with local nighttime. Each circle represents a coherent GW detection at a single triad, color-coded by the amplitude of the beamformed signal. The arrows show the direction of propagation. Station locations are indicated by gray dots. b) Green bins show areas where the TA was deployed but GWs were not detected for this time period. Dark red bins show areas where detections were made.

This method detects any coherent long wavelength signal crossing over a subset of the array, although it will eliminate rare cases of interfering GWs with similar amplitudes. This algorithm detects coherent signals with amplitudes as low as 20 Pa in this band. A separate analysis shows that most of the signals with amplitudes below 60 Pa have a seasonal and diurnal time dependence that clearly distinguishes them from the larger signals and indicates a different origin. We therefore apply a lower threshold of 60 Pa to remove low amplitude signals with a competing physical source mechanism. Although this removes some signals associated with convective activity, as can be seen in Figure 4, we restrict our analysis to larger signals.

We also apply a mask to areas where the rainfall, as defined by the NCEP/EMC precipitation data, is over 2 mm/hr within 30 km of a TA site. The purpose of this mask is to remove regions of heavy rainfall because the high mass of condensate in convective clouds can lead to perturbations in surface pressure on the order of 100 Pa (Bacmeister et al., 2012). For instance, Stephan et al. (2016) observed large, anomalous pressure perturbations in regions where precipitation exceeded 1mm/(10 min). The 2mm/hr threshold was chosen to correspond approximately with this value. The spatial scale distance of the mask corresponds to about half the interstation spacing. After removing the masked areas, the remaining 2-6 hr period signals are identified as GWs.
This algorithm is used to create a catalog of detections that are used to assess the occurrence rate of GWs in the 2-6 hr frequency band observed at Earth's surface, which are then compared with measurements made by the AIRS instrument. The catalog also includes the wave properties of each detected wave.

3.2 GW occurrence frequencies at the Earth's surface

Past studies (including Hoffmann and Alexander, 2010) have revealed a high level of GW activity at local night during the thunderstorm season from May through August (MJJA) in the area to the west of the Great Lakes. The TA crossed this region from 2010-2012 and continued to the east coast by 2014. This study focuses on two time segments of the year during 5-year period; the thunderstorm season from 1 May to 31 August, called MJJA, and the remainder of the year, from 1 September through 30 April of the next year, denoted here by SONDJFMA. Figure 7 shows a comparison of the occurrence rate of GWs over the entire day during MJJA with those made during SONDJFMA. Figure 7 is a compilation of all observations made over the changing network configuration over the duration of this study, The area of GW activity is strongly concentrated in a region to the west of the Great Lakes during the thunderstorm season, with a 30% probability of detecting a GW at least once a day during these months. Coherent GWs are detected over a broader region during the remainder of the year, with a peak occurrence rate of 16%.

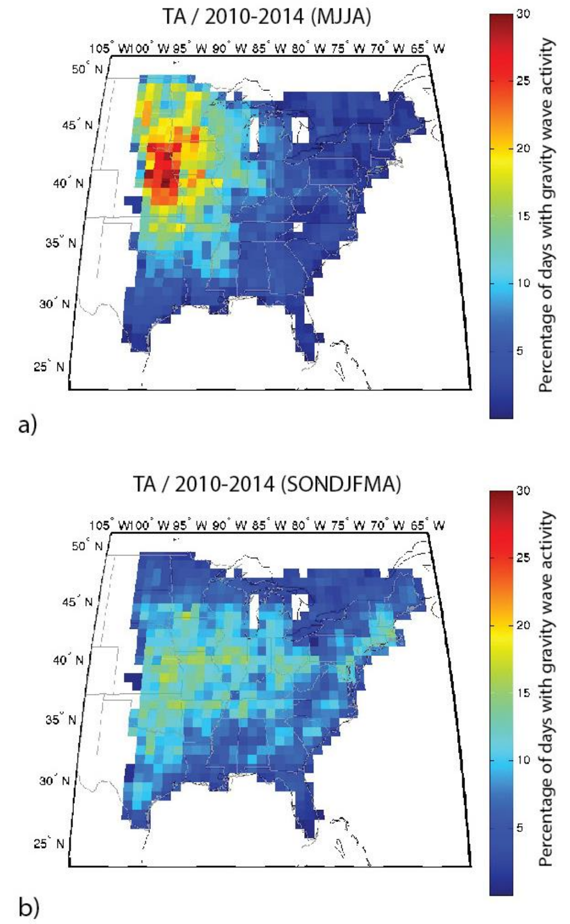

Figure 7. A compilation of the daily mean occurrence rate of GWs in the 2-6 hr frequency band observed at Earth's surface for a) the 4 months from May through August and b) the 8 months from September through April during the 5-year timespan from 2010-2014.

The occurrence rates for the thunderstorm season were further broken down into two six-hour time periods each day - from 03:30-09:30 UT and 15:30 to 21:30 UT - as shown in Figure 8. The first time period spans the local night and is comparable to observations made by the AIRS instrument during the descending orbit. The second period is local daytime and includes the AIRS local daytime overpass. As shown, the occurrence rates differ between the two time periods. Similar to the AIRS observations shown in the next section, GWs are detected at ground-level more frequently at night than during the day, and most detections are made to the west of the Great Lakes. The local night time occurrence rate rises to 17.3% in this area. During the local daytime hours, the occurrence frequency is much less concentrated as shown in Fig. 8b, and reaches a maximum of 8.9%. The percent of time that rainfall exceeds 2 mm/hr during these time intervals, corresponding to data removed from the analysis, is also shown in this figure.

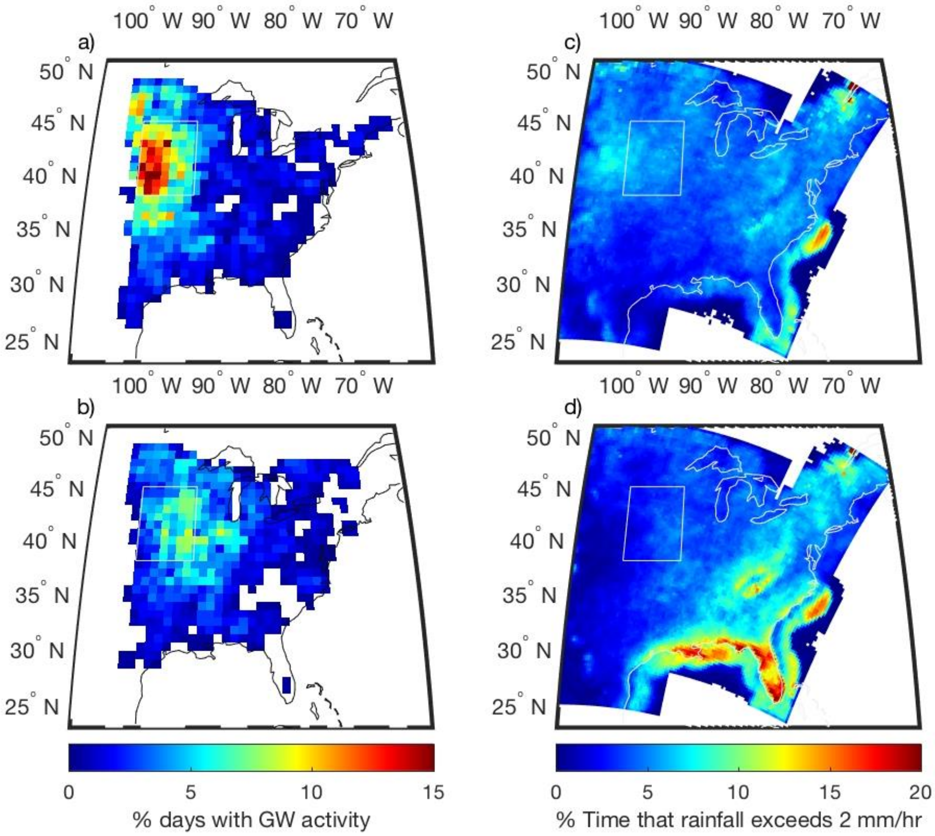

Figure 8. A compilation of occurrence rates of GWs in the 2-6 hr frequency band observed at the Earth's surface during thunderstorm season (May-Aug) during a) local night (03:30-09:30 UT) and b) local day (15:30-21:30 UT). c) and d) show the percentage of time rainfall exceeded 2 mm/hr during the same time intervals. Note that the color scale used on the left is different than in Figure 7. The area outlined in white in each panel is where surface GW activity is a maximum, from 38-45 ^{o}N and 92-99 ^{o}W.

As discussed above, array processing at each triad also gives information on the speed and direction of GW signals and how these quantities vary across the study area. The angle histograms in Figure 9 show the direction of motion for GW detections made in May to August from 2010 through 2014 during local night. For clarity, the detections are grouped over larger areas than in the previous plots; each angle histogram covers a nearly square region of 3^{o} north-south by 3.9^{o} east-west. The angle histograms are polar plots that show the distribution of GW propagation directions, in angular bins of 20^{o}. The length of each bin reflects the number of GWs with a propagation direction in that angular range. The color coding shows the distribution of GW amplitudes for each bin. As shown, most of the detected GW propagate to the east-southeast and their amplitudes are greatest to the west of the Great Lakes, where they are most common. Similarly, Figure 10 shows the angular distribution of phase velocities for GW detections in this same time period. The median phase velocity is 25 m/s. In general, their phase velocities are lower west of the Great Lakes, where amplitudes are highest. Their eastward motion may be due to the fact that rainfall is heaviest just to the west of the GW hotspot, or due to the tropospheric jet stream, which blows eastward throughout the year.

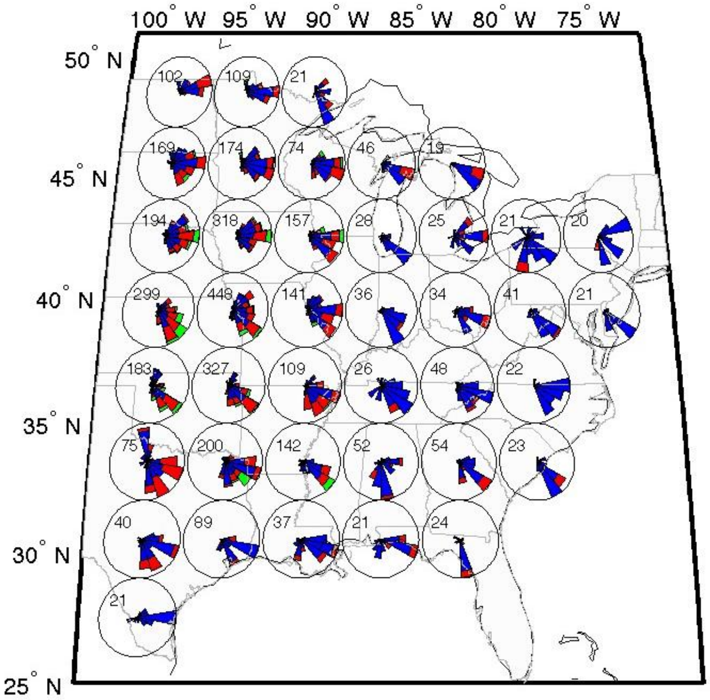

Figure 9. Angle histograms showing direction of propagation and amplitude of coherent waves detected during the thunderstorm seasons, May through August, compiled from 2010-2014. Blue indicates signals with amplitudes from 60 to 100 Pa, red indicates amplitudes from 61-160 Pa, and green indicates larger amplitudes. The total number of detections made for each region are shown to the upper left of each histogram. All detections were made during the local night (from 03:30-09:30 UT). The largest waves are seen to the west of the Great Lakes. Most signals propagate in an eastward direction.

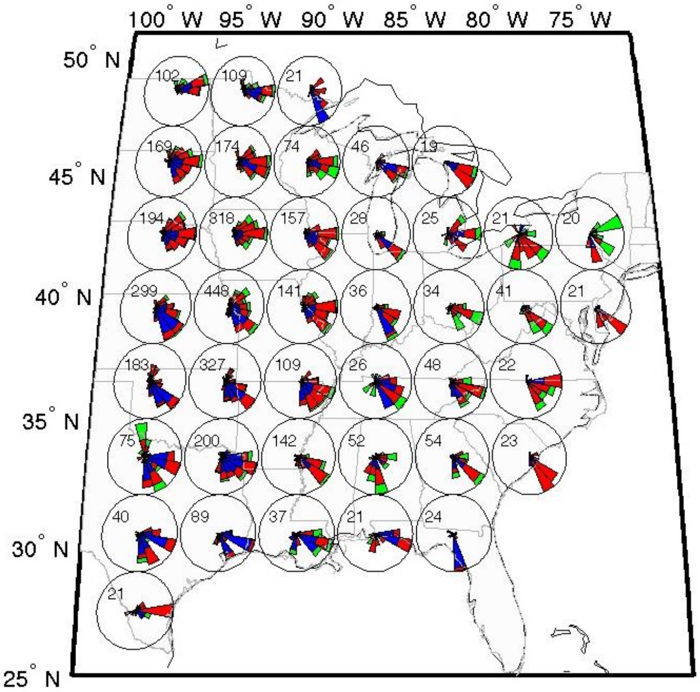

Figure 10. As for Figure 9, but showing phase velocities. Blue indicates signals with velocities up to 25 m/s, red indicates velocities from 25-50 m/s, and green indicates higher velocities.

4. Observations of GWs in the stratosphere and deep convection

Figure 11 shows AIRS occurrence frequencies of stratospheric GWs and convective events over the North American Great Plains during May to August for the years 2010 to 2014. The occurrence frequencies were calculated following the approach outlined by Hoffmann and Alexander (2010) and Hoffmann et al. (2013). GW events are identified if the local variance of the 4.3 μm BT perturbations within a radius of 100 km around each footprint exceeds a threshold that is significantly larger than the measurement noise. Similarly, convective events are identified if the 8.1 μm BT measurement for a footprint drops below a threshold that is indicative for the presence of cold cloud tops related to deep convection in the instrument's field of view. Following Hoffmann et al. (2013), we applied thresholds that depend on latitude, month, and time of day. Hoffmann and Alexander (2010) used a fixed-threshold approach for their study, but we found that the variable-threshold approach used by Hoffmann et al. (2013) generally copes better with varying measurement noise of the AIRS instrument. Typical threshold values at 20-50°N during May to August are in the range of 0.012-0.039 K^2 at daytime and 0.019-0.082 K^2 at nighttime. Occurrence frequencies are calculated from event / non-event counts for individual satellite footprints based on an 0.5° x 0.5° longitude-latitude grid. The analysis is conducted separately for nighttime during the descending parts of satellite orbits, and daytime during the ascending parts of satellite orbits.

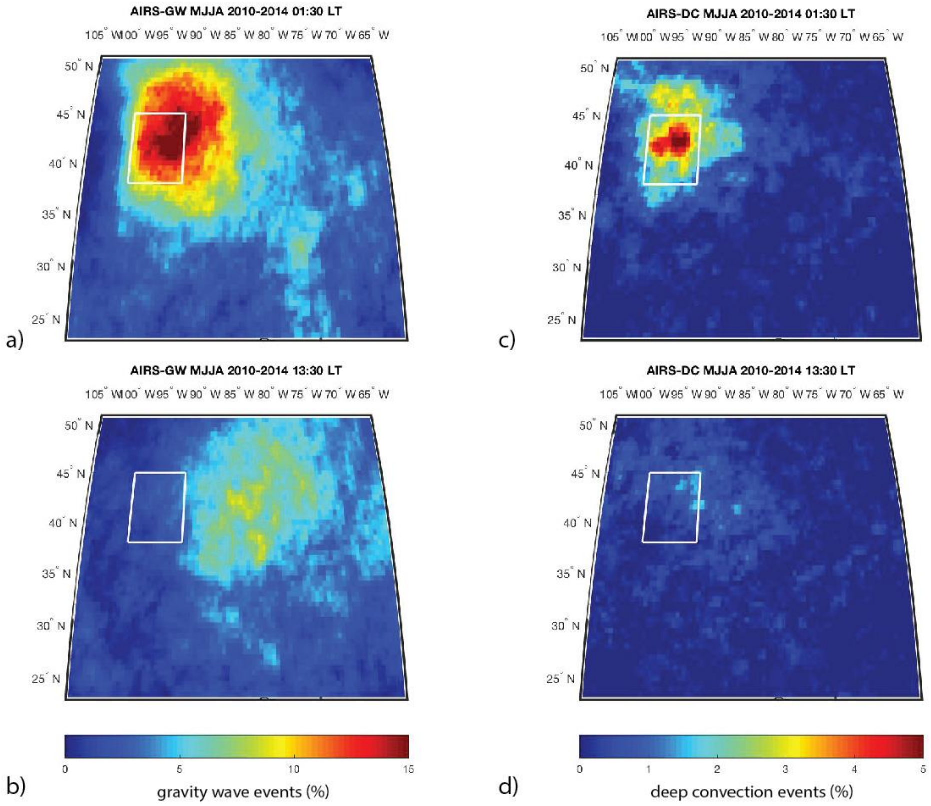

Figure 11. In the left column the occurrence frequency of GWs in the stratosphere is shown over the entire study area from observations made by the AIRS instrument during May through August from 2010 through 2014. Results from descending orbits during the local nighttime, and ascending orbits during the local daytime are shown in (a) and (b) respectively. The panels in the column on the right show the occurrence frequency of deep convection events for the descending and ascending orbits (c and d respectively). The bins in these images are 0.5° on a side. The area outlined in white in each panel is where convective activity at nighttime is a maximum, from 38-45^{o}N and 92-99^{o}W.

The patterns of GW and convective activity found in the AIRS data for the years 2010-2014 in Fig. 11 are quite similar to those reported by Hoffmann and Alexander (2010) for the years 2003-2008. In the nighttime measurements we found significantly increased wave activity (occurrence frequencies of 5-15%) at 35-50°N and 86-98°W, with the maximum of wave activity being found at 40-45°N and 92-96°W. This increase in wave activity is associated with increased convective activity (occurrence frequencies of 2-5%) at 35-50°N and 86-102°W, with a local maximum at 41-44°N and 92-98°W. Hoffmann and Alexander (2010) explained the eastward shift of the GW maximum with respect to the convective maximum based on predominant eastward propagation (cf. Figure 3) and better observability of eastward propagating waves by AIRS. At daytime, the hotspot of convective wave activity over the North American Great Plains is still visible, but occurrence frequencies of both convection and GWs are much lower than at nighttime. This is attributed to the diurnal cycle of convection, which relates to mesoscale convective systems intensifying over the Great Plains at night in the summer thunderstorm season [e.g. Carbone and Tuttle, 2008]. We found that convective wave activity outside the thunderstorm season (from September to April) is relatively weak (not shown).

5. Joint observations of GWs in the stratosphere and Earth's surface

The array analysis method used to detect GWs at the Earth's surface measures the time rate-of-change of long period pressure signals crossing the TA, while GWs in the stratosphere are identified by computing the spatial variation of the BT for a given orbit. It is notable that, using these very different instruments and analysis methods over the five year study period, GW occurrence frequencies at the Earth's surface, shown in Figure 8, show similar spatial and temporal patterns as at stratospheric altitudes, shown in Figure 11. However, the array analysis method described in Section 3 does not allow for a direct day-to-day comparison of GW activity at the ground and in the stratosphere. For this, we compute the spatial pressure variations measured by TA barometers at given times and compare these to the spatial 4.3 μm BT variances which serve as a proxy for GW activity in the stratosphere. The spatial pressure variances in the 2-6 hr band are computed hourly over a given region to obtain a measure of the GW activity As before, data at any station are masked when the peak precipitation exceeds 2 mm/hr. We also computed the hourly total rainfall within this region.

Our analysis aims to identify whether GWs in the two data sets are likely related to the same convective activity, and the degree of correlation between the rainfall and pressure variances. The region of interest chosen for this day-to-day comparison of AIRS and TA GW observations, and the rainfall, is to the west of the Great Lakes, from 38-45°N and 92-99°W which captures the zones of most intense gravity and convective wave activity for the AIRS measurements, as well as the GW region captured by the TA pressure measurements. Within this region of interest, we note that the AIRS GW maximum is slightly further east than the TA region because waves observed by AIRS in the stratosphere systematically propagate further east from their source, while waves seen at the surface may appear closer to their source. The time interval is from 1 May to 31 August, 2011, which includes the thunderstorm season for the year that the TA had the greatest coverage of the region of interest. Figure 12 shows a comparison of observations from the AIRS sensor and the TA pressure sensors, and the precipitation statistics. Figure 12a shows the minimum BT at 8.1 μm for each pass across the region of interest; low values for these measurements are considered a proxy for convective activity. The European Centre for Medium-Range Weather Forecasts (ECMWF) ERA-Interim reanalysis 6-hourly zonal and meridional winds at an altitude of about 35 km are shown in Figure 12b. Figure 12c shows the noise corrected variance of BT perturbations at 4.3 μm, which is a proxy for GW activity in the stratosphere. In Figures 12a and 12c, the nighttime measurements are shown in red; the daytime values are shown in green. Figure 12c shows that the four largest GW events during the thunderstorm season in 2011 occurred during local night on the dates of 18 June, 20 June, 27 June, and 11 July, 2011. Figure 12d shows the total precipitation within the the study area for the TA, computed hourly, and the pressure variances within this same region. The four dates of greatest activity in the stratosphere are marked in the lowest panel by the green lines.

There is considerable agreement between ground and satellite observations, particularly linking convective storm activity to the pressure variance at the Earth's surface. A visual inspection of Figs 12a and 12d indicates that periods of high convective activity, marked by low 8.1 μm BT measurements, are concurrent with periods of high pressure variances measured at the TA. To obtain a quantitative assessment, we compute the Spearman rank-order coefficient r_s and Pearson linear correlation coefficient r_p. Both coefficients range between -1, indicating a negative correlation and +1, indicating positive correlation, with values near zero indicating that the pairs of variables are uncorrelated. The Spearman rank correlation coefficient, which considers the ranking of the data points rather than their absolute values, is the more robust measure of correlation as it is less sensitive to outliers. Spearman's correlation is sensitive to almost any monotonic correlation in the data, whether linear or not. Tests of the statistic significance, which is a measure of the probability that the observed coefficient would occur for the null hypothesis, exist for both the Pearson and Spearman tests. We have taken into account estimates of the data (Zülicke and Peters, 2010) to estimate the effective degrees of freedom and to compute the significance of each of the derived correlation coefficients. More details on these statistical measures can be found in Press et al. (2002).

Comparing the AIRS observations of 8.1 μm BT values to the pressure variance values with no time lag for the 2011 thunderstorm season, we find that r_s for the nighttime passes is -0.58 with a significance value of 0.002, indicating significant correlation. The Pearson r_p value is -0.36, indicating a moderate linear correlation. The negative correlation values imply that higher levels of convective activity, as indicated by low 8.1 μm BTs, correlate to higher levels of GW activity near the surface, as expected. The corresponding values for the daytime passes are low, indicating little correlation. These correlation values are for direct temporal correlations, and do not take into account any time lag between GWs observed at the Earth's surface and convective storm activity as measured by the AIRS instrument. Because the TA data have a high time sampling rate, we can cross-correlate pressure variance values and the AIRS measurements as a function of time. We find that correlation values for nighttime passes peak between zero to one hour after the satellite pass, indicating a very small time-lag between convective activity and the corresponding surface GW activity. The correlation values tend to decrease sharply after a two hour time delay. This pattern holds for daytime passes as well, with peak correlation from zero to one hour after the satellite pass, and correlations decreasing after a two hour lag. Comparison of the hourly precipitation with the pressure variances indicates a much lower correlation, with $r_s = 0.22$, but with significance values of approximately .16, indicating that this correlation may not be significant. The Pearson statistic also indicates a poor correlation.

The link between GW activity at the ground and in the stratosphere appears weaker. To make such a comparison first requires consideration of the stratospheric winds (Fig. 12b), because waves are generally only visible to AIRS sensors when those winds are strong. So we focus on the June-August period. Within that period, a visual inspection of Figs 12c and 12d indicates that three of the days identified as being highly active in the stratosphere (18 June, 20 June and 27 June in Figure 12c) are also active on the ground.

This is particularly true on June 27, discussed earlier. The fourth highly active day in the AIRS timeseries, 11 July, is not unusually active on the ground. There are several other days earlier and later in the thunderstorm season during which the pressure variances are considerably greater than the background level, but the 4.3 μm BT variance is not much enhanced in the AIRS timeseries for these days. The analytic measures of correlation between the 4.3 μm BT variance and the pressure variance measurements on the ground are much higher for nighttime satellite passes than for the day. The Spearman r_s value peaks at 0.42 from zero to one hours after the night-time satellite pass, with significance values indicating significant correlation. The correlations decrease significantly after several hours. The Pearson r_p values for zero to 1 hour time delays are approximately 0.56, indicating significant linear correlation. Correlation values for daytime passes are insignificant. This is likely due to the lack of GW activity in the stratosphere in this region, as shown in figure 10b. We note that these comparisons were made for the entire thunderstorm season, regardless of the strength of the zonal wind; Alexander and Barnet (2007) report that stationary orographic GWs are detected by AIRS only when horizontal winds exceed about 40 m/s, which is attributed to the observational filter effect. For travelling waves from convection, this threshold will be lower: we estimate closer to 10 m/s. This wind effect can also be seen by comparing Figs. 12b and 12c.

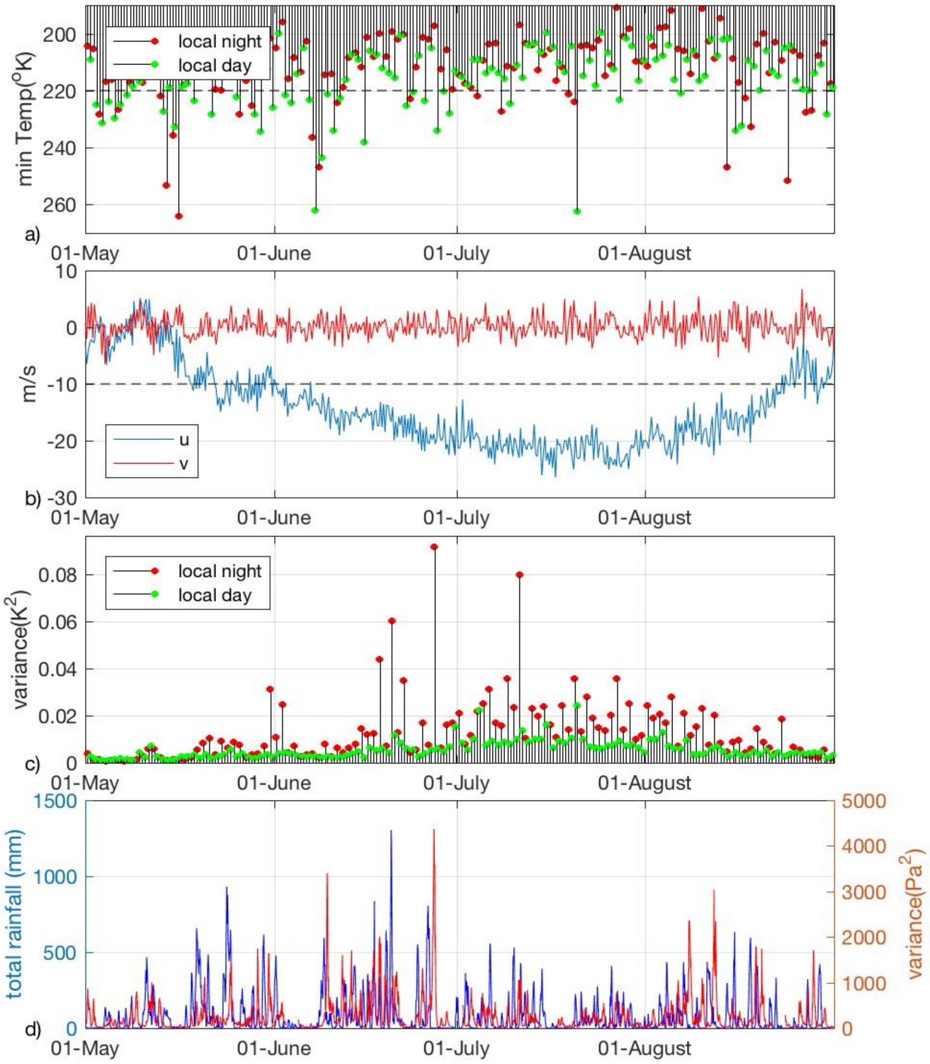

Figure 12. A comparison of observations from the AIRS sensor and the TA pressure sensors, and the precipitation statistics for 1 May 1 through 31 August, 2011 in the region from 38-45^{o}N and 92-99^{o}W. a) The AIRS minimum BT at 8.1 µm, which is a proxy for convective storm activity. Values from the ascending branch (local daytime measurements) are shown in green; red dots indicate values from the descending branch (local night time). A dashed line at 220K is a typical threshold for detecting deep convection is used here as in Hoffmann and Alexander (2010); a variable-threshold approach is used here and in Hoffmann et al. (2013). b) ERA-Interim zonal and meridional winds at ~35 km altitude at 6 hour time intervals. The dashed line at 10 m/s marks the stratospheric wind speed; AIRS detections of GWs are not expected at lower wind speeds. c) The variance of AIRS 4.3 µm BT perturbations, which is a proxy for GW activity in the stratosphere. The values for plots a), b) and c) are taken over the rectangular region from 41-44°N, 92-98°W. d) The total hourly rainfall in this region (blue), and the variance of pressure perturbations in the 2-6 hr band (red) at Earth's surface. Pressure variance was computed after excluding stations at times when maximum precipitation exceeded 2 mm/hr.

Figure 13 shows the diurnal fluctuation in the variance of recorded pressure in the 2-6 hr band in two regions of the study area, and over separate time spans. As shown in Figure 8a, GWs are most frequently detected during the local night to the west of the Great Lakes during the thunderstorm season. Most of the activity is concentrated from 38-45°N and 92-99°W. The mean pressure variance in this region, computed hourly for MJJA of 2011, is shown by the heavy black dotted curve in Figure 13. The mean rainfall in this area for this same time interval is shown by the heavy blue dotted line. The solid black curve represents the mean pressure variance in a less active region 10° to the east, from 38-45°N and 82-89°W for MJJA of 2013. The mean rainfall for this area is shown by the solid blue line. While the AIRS observations are made only twice per day at 0828 and 1929 UT plus or minus 23 minutes for each orbit, the TA recordings are made continuously through the day, allowing us to examine the GW variations in much greater detail. The nighttime AIRS observation (at approximately 0828 UT) occurs near a time of maximum GW activity on the ground. The daytime pass occurs shortly before the time of minimum activity. Little GW activity is seen in the eastern region and any diurnal variations are weak.

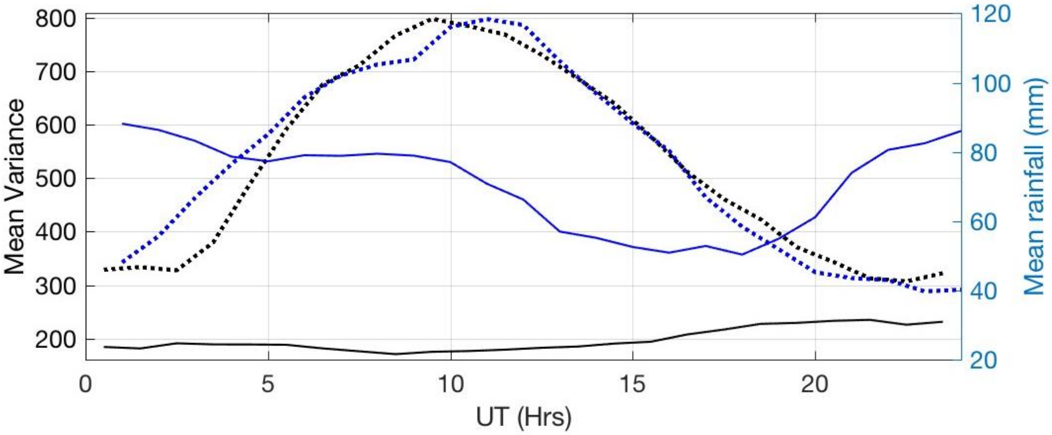

Figure 13. Mean TA pressure variance (Pa^2) and total rainfall per hour in two rectangular regions near the Great Lakes during the thunderstorm season, MJJA. The heavy dashed curves represents observations from 38-45°N and 92-99°W; black is the mean hourly pressure variance in 2011, blue is the average total rainfall during this same period. The solid curves are from observations made in the same latitude range in 2013 but in the much less active area from 82-89°W, with black and blue lines representing the pressure variance and total rainfall, respectively.

6. Discussion and conclusions

The locus of GW hotspot observed at the Earth's surface in this study is consistent with previous observations of mesoscale pressure perturbations in the US. Koppel et al. (2000) identified a concentration of large pressure variations (> 425 Pa) west of the Great Lakes, in the lee of the Rocky Mountain ranges; these perturbations were associated with cyclones. However, that study found that over a 25 year period over the conterminous US, GW activity peaked at noon LT and exhibited a broad minimum from August through November. A prominent region of mesoscale pressure perturbations was also found in this area by Jacques et al. (2015, 2017). This feature was particularly prominent during the spring and summer months (Jacques et al., 2015). Mesoscale pressure perturbations over the Great Central Plains with large amplitudes (>100 Pa) and areal extents (>10,000 km^2) were tracked by Jacques et al. (2017); their eastward motion and speeds are consistent with the GW phase velocities and propagation azimuths in this study.

GW detections made at the Earth's surface exhibit the same broad patterns as observed at stratospheric altitudes by the AIRS sensor (e.g. Figs. 8 and 11). However, we note that due to the movement of the TA over the duration of the study period, the western areas are sampled in earlier years than the eastern areas. It is possible that the lower level of GW activity to the east reflects a decrease in GW with time, rather than a spatial variation. Indeed, Figure 14 shows variations in GW activity sensed by the AIRS instrument over the course of this 5-year study. The level of activity in the stratosphere to the west of the Great Lakes was relatively high in 2010, 2011 and in 2014. There was a lull in activity in 2012 and 2013, which is mirrored in the year by year variations in the deep convective activity (not shown) The decrease in activity in the stratosphere to the west of the Great Lakes that occurred between 2011 and 2012 is particularly striking, and important for this study given that the TA network was located in that area at that time. In addition, each station in the network was deployed for two years and therefore recorded data during two consecutive thunderstorm seasons. Figure 15 shows a decrease in GW activity detected by the TA from 2011 to 2012 - paralleling what is seen in the AIRS data. This is consistent with a study by Jacques et al. (2015) that observed a decline in mesoscale pressure perturbations on TA sensors after August 2011. The 2012 data also indicate that despite the overall lower GW occurrence rate, a decline in activity can still be observed from the western edge of the network (located where the GW activity was concentrated in 2011) to the eastern edge of the network. The data suggest that the level of activity observed on the ground varied from year to year as it did in the stratosphere. We note that the region of highest GW activity within the stratosphere is displaced slightly to the east of the corresponding region at ground level. The event shown in Figure 3a offers a possible explanation of this shift. The region where the 4.3 μm BT variances are greatest is located east of the convective source because of horizontal propagation of the waves and filtering effect of the background winds. This suggests that the GW hotspot detected at ground level by the TA coincides with the convective source point of GWs observed by AIRS.

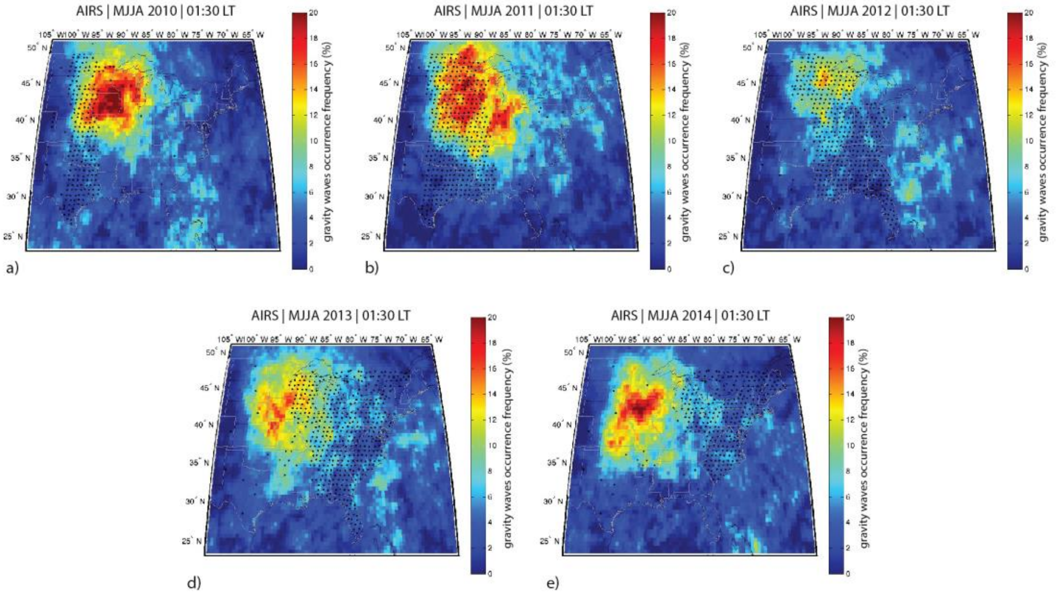

. **Figure 14**. Year to year variability of gravity wave occurrence in the stratosphere during the thunderstorm season (MJJA) from observations made by the AIRS sensor during local nighttime, descending orbits. The small black dots represent stations within the TA and show the movement of the network through the years.

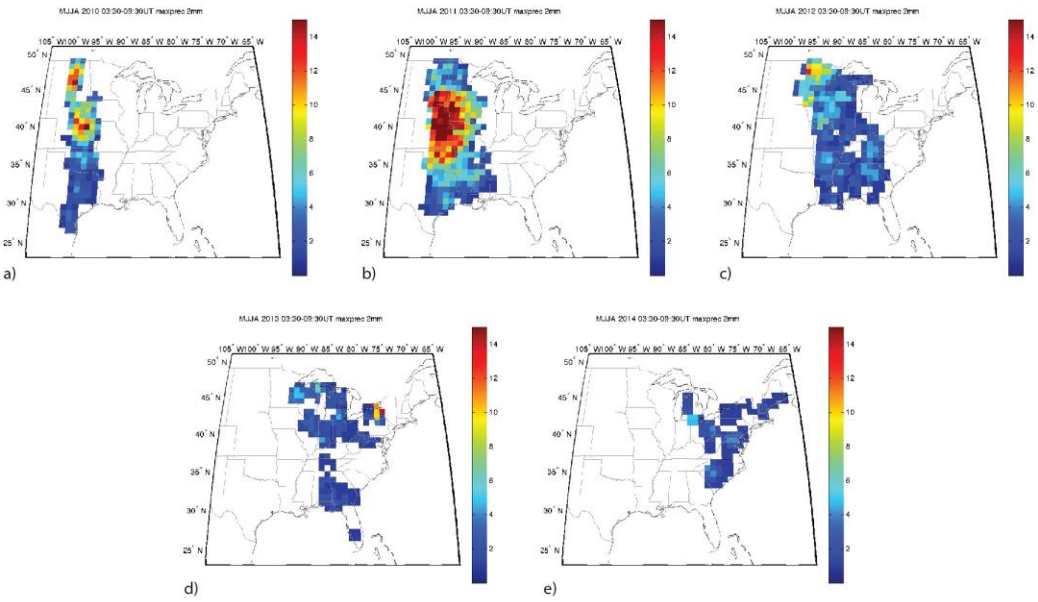

.

. **Figure 15.** Year to year variability of gravity wave occurrence at ground level during the thunderstorm season (MJJA) from 03:30-09:30 UT. This time range includes the times shown in Figure 14. The region sampled changes from year to year due to the gradual eastward movement of the TA. Data recorded at times when precipitation exceeded 2 mm/hr were excluded from these plots.

Seasonal and diurnal changes in GW activity observed in the two datasets are also consistent. As seen in Figure 7, the level of activity on the ground varies seasonally (with a surge in activity during the thunderstorm season) as it does in the stratosphere (Hoffmann and Alexander, 2010). In Figure 8, the day/night differences at ground level also mirror those observed in the stratosphere (Figure 11). In summary, although the integrated results from 5 years of TA data cannot show in an absolute sense how GW activity varied at ground-level spatially across the study area, they strongly suggest that it is concentrated to the west of the Great Lakes and occurs mainly at nighttime during the thunderstorm season, similar to the AIRS results.

Expanding on the conclusions of the Stephan et al. (2016) case study, the agreement between the AIRS and TA datasets strongly suggests that convection is the common origin between GW observations at ground level and in the stratosphere. The time series shown in Figure 12 permitted a quantitative assessment of the temporal linkage between GWs observed at ground level and both the level of GW activity in the stratosphere and the convective activity observed by satellite, during the thunderstorm season in 2011. The correlation between GWs observed at the TA and convective activity observed by AIRS is higher at night than during the day, but both are considered statistically significant. The 2-6 hr pressure variance at ground level, which is the proxy for GWs at ground level, was computed once every hour. With this sampling rate there is no discernable time lag between the two. Based on these observations, we conclude that GWs at the ground level are due to mesoscale convective systems. In previous studies (Hoffmann and Alexander, 2010; Grimsdell et al., 2010; Stefan and Alexander, 2015) it was established that the stratospheric GWs were also caused by convection. We conclude that convective activity to the west of the Great Lakes is the dominant source of GWs both at ground level and within the stratosphere. Day-to-day correlations between GWs in the stratosphere and at ground level are poorer, and only statistically significant at nighttime. Little GW activity is detected in the stratosphere at times when the zonal winds are weak, as expected, since these waves are not expected to be detected by AIRS (Alexander and Barnet, 2007).

One other important difference between TA and AIRS datasets is that TA observations are sampled once per second while AIRS samples the region just twice per day. Any diurnal variations in GWs can therefore be examined in much greater detail at ground level - although as seen in Figure 13 the two AIRS passes are quite well timed to examine GW occurrence near its peak and minimum. The TA data show that at ground-level in the smaller study area to the west of the Great Lakes there is a smooth, sinusoidal change in the frequency of GW occurrence during the thunderstorm season each day. Comparison of this result with the corresponding result from the equal-sized region to the south of the Great lakes indicates that this diurnal trend is not ubiquitous. The diurnal change observed in this second area is relatively weak and does not reach its peak at night time.

Acknowledgements

This material is based upon work supported by the National Science Foundation under Grant Nos. EAR-1358520 and AGS-1519271. This study benefited greatly from services provided by the Array Network Facility (ANF) at UC San Diego and the Incorporated Research Institutions for Seismology (IRIS) Data Management Center (DMC). The barometric pressure data are available to the public at the Iris Data Management Center at http://ds.iris.edu/dms/. Funding for the atmospheric sensors in the TA was provided by NSF. AIRS data products are distributed by the NASA Goddard Earth Sciences Data Information and Services Center. ERA-Interim data were obtained from the European Centre for Medium-Range Weather Forecasts. Climate Prediction Center/National Centers for Environmental Prediction/National Weather Service/NOAA/U.S. Department of Commerce, and Joint Office for Science Support/University Corporation for Atmospheric Research, 2000: NCEP/CPC Four Kilometer Precipitation Set, Gauge and Radar. Research Data Archive at the National Center for Atmospheric Research, Computational and Information Systems Laboratory, Boulder, CO. [Available online at http://rda.ucar.edu/datasets/ds507.5/.] Accessed 26 Jul 2016. We thank the reviewers for constructive comments.

References

Alexander, M. J., and C. Barnet, 2007: Using satellite observations to constrain parameterizations of gravity wave effects for global models, J. Atmos. Sci., 64, 1652-1665.

Alexander, M. J. and Pfister, L., 1995, Gravity wave momentum flux in the lower stratosphere over convection, Geophys. Res. Lett., 22, 2029–2032.

Alexander, M. J. and Rosenlof, K. H., 1996, Nonstationary gravity wave forcing of the stratospheric zonal mean wind, J. Geophys. Res., 101, 23465–23474.

Aumann, H. H., Chahine, M. T., Gautier, C., Goldberg, M. D., Kalnay, E., McMillin, L. M., Revercomb, H., Rosenkranz, P. W., Smith, W. L., Staelin, D. H., Strow, L. L., and Susskind, J., 2003, AIRS/AMSU/HSB on the Aqua Mission: Design, Science Objective, Data Products, and Processing Systems, IEEE T. Geosci. Remote Sens., 41, 253–264.

Bacmeister, J. T., P. H. Lauritzen, A. Dai, and J. E. Truesdale, 2012: Assessing possible dynamical effects of condensate in high resolution climate simulations. Geophys. Res. Lett., 39, L04806, doi:10.1029/2011GL050533.

Bosart L. F. and J. P. Cussen, 1973: Gravity Wave Phenomena Accompanying East Coast Cyclogenesis. *Mon. Wea. Rev.*, 101, 446-454

Brunk, I. W., 1949: The Pressure Pulsation of 11 April 1944. *J. Meteorology*, 6, 395-401.

Busby, R.W., Vernon, F.L., Newman, R.L. & Astiz, L., 2006. Earth-Scope’s USArray: advancing eastward, EOS, Trans. Am. Geophys. Un., 87(52), Fall Meet. Suppl., Abstract U41B-0820.

Cansi, Y., 1995. An automatic seismic event processing for detection and location: the P.M.C.C. method, Geophys. Res. Lett., 22, 1021–1024.

Carbone, R. E., and J. D. Tuttle, 2008, Rainfall Occurrence in the U.S. Warm Season: The Diurnal Cycle, J. Climate, 21, 4132-4146.

Chahine, M. T., Pagano, T. S., Aumann, H. H., Atlas, R., Barnet, C., Blaisdell, J., Chen, L., Divakarla, M., Fetzer, E. J., Goldberg, M., Gautier, C., Granger, S., Hannon, S., Irion, F. W., Kakar, R., Kalnay, E., Lambrigtsen, B. H., Lee, S., Marshall, J. L., McMillan, W. W., McMillin, L., Olsen, E. T., Revercomb, H., Rosenkranz, P., Smith,W. L., Staelin, D., Strow, L. L., Susskind, J., Tobin, D., Wolf, W., and Zhou, L., 2006, AIRS: improving weather forecasting and providing new data on greenhouse gases, B. Am. Meteorol. Soc., 87, 911–926.

Choi, H. J., Chun, H. Y., Gong, J., and Wu, D. L., 2012, Comparison of gravity wave temperature variances from raybased spectral parameterization of convective gravity wave drag with AIRS observations, J. Geophys. Res., 117, D05115, doi:10.1029/2011JD016900.

de Groot-Hedlin, C.D., and Hedlin, M.A.H., 2014, Infrasound detection of the Chelyabinsk meteor at the USArray, Earth Planet. Sci. Lett. DOI: 10.1016/j.epsl.2014.01.031

de Groot-Hedlin, C.D., Hedlin, M.A.H. and Walker, K.T., 2014, Detection of gravity waves across the USArray: A case study, *Earth Planet Sci. Lett.*, DOI: 10.1016/j.epsl.2013.06.042

de Groot-Hedlin, C.D. and Hedlin, M.A.H., 2015, A method for detecting and locating geophysical events using clusters of arrays, *Geophys. J. Int*., v203, 960-971, doi: 10.1093/gji/ggv345.

Eckermann, S. D., Wu, D. L., Doyle, J. D., Burris, J. F., McGee, T. J., Hostetler, C. A., Coy, L., Lawrence, B. N., Stephens, A., McCormack, J. P., and Hogan, T. F., 2006, Imaging gravity waves in lower stratospheric AMSU-A radiances, Part 2: Validation case study, Atmos. Chem. Phys., 6, 3343–3362, doi:10.5194/acp-6-3343-2006.

Eom, J. K., 1975: Analysis of the Internal Gravity Wave Occurrence of 19 April 1970 in the Midwest. *Mon. Wea. Rev.*, 103, 217-226

Gong, J., Wu, D. L., and Eckermann, S. D., 2012, Gravity wave variances and propagation derived from AIRS radiances, Atmos. Chem. Phys., 12, 1701–1720, doi:10.5194/acp-12-1701-2012.

Grimsdell, A. W., Alexander, M. J., May, P. T., and Hoffmann, L., 2010, Model study of waves generated by convection with direct validation via satellite, J. Atmos. Sci., 67, 1617–1631.

Grivet-Talocia, S., and F. Einaudi, 1998: Wavelet analysis of a microbarograph network. IEEE Trans. Geosci. Remote Sens., 36, 418–433, doi:10.1109/36.662727.

Grivet-Talocia, S., F. Einaudi, W. L. Clark, R. D. Dennett, G. D. Nastrom, and T. E. VanZandt, 1999: A 4-yr climatology of pressure disturbances using a barometer network in central Illinois. Mon. Wea. Rev., 127, 1613–1629, doi:10.1175/1520-0493(1999)127<1613: AYCOPD>2.0.CO;2.

Havskov, J. & Ottemöller, L., 2010. Routine Data Processing in Earthquake Seismology, Springer.

Hoffmann, L. and Alexander, M.J., 2010, Occurrence frequency of convective gravity waves during the North American thunderstorm season, *Journal of Geophysical Research: Atmospheres*, v115, doi: 10.1029/2010JD014401.

Hoffmann, L., Xue, X. and M.J. Alexander, 2013, A global view of stratospheric gravity wave hotspots located with Atmospheric Infrared Sounder observations, *Journal of Geophysical Research: Atmospheres*, v118, 416-434, doi: 10.1029/2012JD018658.

Hoffmann, L., Alexander, M. J., Clerbaux, C., Grimsdell, A. W., Meyer, C. I., Rößler, T., and Tournier, B., 2014, Intercomparison of stratospheric gravity wave observations with AIRS and IASI, Atmos. Meas. Tech., 7, 4517–4537, doi:10.5194/amt-7-4517-2014.

Jacques, A. A., J. D. Horel, E. T. Crosman, and F. L. Vernon, 2015, Central and eastern U.S. surface pressure variations derived from the USArray network. Mon. Wea. Rev., 143, 1472–1493, doi:10.1175/MWR-D-14-00274.1.

Jacques, A. A., J. D. Horel, E. T. Crosman, F. L. Vernon, and J. Tytell, 2016, The Earthscope US Transportable Array 1 Hz surface pressure dataset. Geosci. Data J., 3, 29–36, doi:10.1002/gdj3.37.

Jacques, A. A., J. D. Horel, E. T. Crosman, and F. L. Vernon, 2017, Tracking mesoscale pressure perturbations using the USArray transportable array, Mon. Wea. Rev., 145, 3119-3142, doi:10.1175/MWR-D-16-0450.1.

Koch, S. E., and C. O'Handley, 1997: Operational forecasting and detection of mesoscale gravity waves. Wea. Forecasting, 12, 253–281, doi:10.1175/1520-0434(1997)012<0253:OFADOM>2.0.CO;2.

Koch, S. E.,and S. Saleeby, 2001: An automated system for the analysis of gravity waves and other mesoscale phenomena. Wea. Forecasting, 16, 661–679, doi:10.1175/1520-0434(2001)016<0661: AASFTA>2.0.CO;2.

Koppel, L. L., L. F. Bosart, and D. Keyser, 2000: A 25-yr climatology of large-amplitude hourly surface pressure changes over the conterminous United States. Mon. Wea. Rev., 128, 51–68, doi:10.1175/1520-0493(2000)128<0051:AYCOLA>2.0.CO;2.

Larsen, M. F., W. E. Swartz, and R. F. Woodman, 1982: Gravity-wave generation by thunderstorms observed with a vertically-pointing 430 MHZ radar. *Geophys. Res. Lett.*, 9, 571-574.

Mapes, B. J., 1993: Gregarious Tropical Convection. *J. Atmos. Sci*., 50, 2026-2037.

Pfister, L., Starr, W., Craig, R., Loewenstein, M., and Legg, M., 1986, Small-Scale Motions Observed by Aircraft in the Tropical Lower Stratosphere: Evidence for Mixing and its Relationship to Large-Scale Flows, J. Atmos. Sci., 43, 3210–3225.

Press, W. H., S. A. Teukolsky, W. T. Vetterling, and B. P. Flannery (2002), Numerical Recipes in C: The Art of Scientific Computing, vol. 1, 2nd ed., Cambridge Univ. Press.

Preusse, P., Eckermann, S. D., and Ern, M., 2008, Transparency of the atmosphere to short horizontal wavelength gravity waves, J. Geophys. Res., 113, D24104, doi:10.1029/2007JD009682.

Sato, K., C. Tsuchiya, M. J. Alexander, and L. Hoffmann, 2016: Climatology and Enso-related interannual variability of gravity waves in the Southern Hemisphere subtropical stratosphere revealed by high-resolution AIRS observations. *J. Geophys. Res. Atmos.*, 121, 7622—7640, doi: 10.1002/2015JD024462.

Scaife, A. A., Butchart, N., Warner, C. D., Stainforth, D., and Norton, W., 2000, Realistic quasi-biennial oscillations in a simulation of the global climate, Geophys. Res. Lett., 27, 3481–3484.

Stephan, C. C. and M. J. Alexander, 2015, Realistic simulations of atmospheric gravity waves over the continental U.S. using precipitation radar data. J. Adv. Model. Earth Syst.,07, doi:10.1002/2014MS000396.

Stephan, C.C., Alexander, M.J., Hedlin, M.A.H., de Groot-Hedlin, C.D. and Hoffmann, L., 2016, A case study on the far-field properties of propagating tropospheric gravity waves, *Monthly Weather Review*, 144, 2947-2961, DOI: 10.1175/MWR-D-16-0054.1.

Stobie, J. G., F. Einaudi and L. W. Uccellini, 1983: A Case Study of Gravity Waves—Convective Storms Interaction: 9 May 1979. *Mon. Wea. Rev.*, 40, 2804-2830.

Tepper, M., 1954: Pressure Jump Lines In Midwestern United States, January– August 1951. U.S. Weather Bureau Research Paper No. 37, 70 pp

Tsuchiya, C., K. Sato, M. J. Alexander, and L. Hoffmann, 2016: MJO-related intraseasonal variation of gravity waves in the Southern Hemisphere tropical stratosphere revealed by high-resolution AIRS observations. *J. Geophys. Res. Atmos.*, 121, 7641—7651, doi:10.1002/2015JD024463.

Tytell, J. Vernon, F., Hedlin, M.A.H., de Groot-Hedlin, C.D., Reyes, J., Busby, B., Hafner, K. and Eakins, J. 2015, The USArray Transportable Array as a Platform for Weather Observation and Research, *Bulletin of the American Meteorological Society*, http://dx.doi.org/10.1175/BAMS-D-14-00204.1.

Uccellini, L. W., 1975: A case study of apparent gravity wave initiation of severe convective storms. *Mon. Wea. Rev.*, 103, 497-513.

Wu, D. L., P. Preusse, S. D. Eckermann, J. H. Jiang, M. de la Torre Juarez, L. Coy, and D. Y. Wang, 2006: Remote sounding of atmospheric gravity waves with satellite limb and nadir techniques. *Adv. Space Res.*, 37, 2269-2277.

Yue, J., Thurairajah, B., Hoffmann, L., Alexander, M. J., Chandran, A., Taylor, M. J., Russell III, J. M., Randall, C. E., and Bailey, S. M., 2014, Concentric gravity waves in polar mesospheric clouds from the Cloud Imaging and Particle Size experiment, J. Geophys. Res., 119, 5115–5127, doi:10.1002/2013JD021385.

Zülicke, C. & D. H. W. Peters, 2010: On the estimation of persistence in geophysical time series. Eur. Phys. J. - Special Topics 187: 101 - 108, doi:10.1140/epjst/e2010-01275-2.